

Dynamics of Magnetic Flux Tubes in an Advective Flow Around Black Hole



Arnab Deb

Abstract Observational studies in the two spectral regions of the electromagnetic spectrum, in the domain of the hard X-rays on one hand, and in the domain of radio wavelengths on the other hand, revealed the existence of new stellar sources of relativistic jets known as micro-quasars (Mirabel et al. *Nature* 358(6383):215–217, 1992; Mirabel and Rodriguez, *Nature* 371(6492):46–48, 1994). It is seen that the relativistic jets with significant matter content are produced when the inner part of the disk is destroyed and evacuated (Chakrabarti and D’Silva, *ApJ* 424:138, 1994; Nandi et al. *Astron. Astrophys.* 380:245–250, 2001). Clearly, magnetic field has to play a major role in origin, acceleration and collimation of these relativistic jets. Due to predominantly rotating accretion flows close to the inner edge of a disk, entangled magnetic fields advected through the flow would be toroidal. This is particularly true for weakly viscous, low angular momentum transonic or advective discs. We focus our study to the trajectories of toroidal flux tubes inside a geometrically thick flow which undergoes a centrifugal force supported shock and also the effects of these flux tubes on the dynamics of the inflow and the outflow. Finite difference method (Total Variation Diminishing) is used for this purpose and specifically focussing on whether these flux tubes significantly affect the properties of the outflows such as its collimation and the rate. It is seen that depending upon the cross-sectional radius of the flux tubes which control the drag force, these field lines may move towards the central object or oscillate vertically before eventually escaping out of the funnel wall (pressure zero surfaces) along the vertical direction. A comparison of results obtained with and without flux tubes show these flux tubes indeed could play pivotal role in collimation and acceleration of jets and outflows.

A. Deb (✉)

S.N. Bose National Centre for Basic Sciences, Salt Lake, Kolkata, India

1 Introduction

The process in which matter due to gravity accumulates in the vicinity of a compact object is called accretion. In case of black holes, the inner boundary condition states that matter must fall onto the black hole with velocity of light and this requires all the accretion flow to be transonic in nature. The centrifugal pressure causes the inflowing matter to slow down and this results in piling up of the matter near the inner part of the disk causing an increase in temperature and the matter is puffed up creating a torus like structure. This structure is called the Centrifugal Pressure supported Boundary layer or CENBOL ([4], hereafter C89, 1999, [5]; MLC94, [6]; [7]). As shown by MLC94, in the limit of no radial velocity, the CENBOL has a property similar to as that of a thick accretion disk [35]. Due to this CENBOL region, a fraction of inflowing matter gets ejected as the outflow and this outflow eventually gets collimated and accelerated creating relativistic jets. However, a clear understanding of formation, acceleration, and collimation of these jets has been eluding the astrophysicists. Early theoretical approach to study collimation and acceleration of jets consisted of studies of thin as well as geometrically thick accretion discs as it was believed that the properties of accretion discs are somehow connected to the origin of bipolar jets. Numerous theoretical models [1, 2, 8, 21, 27, 28] showed that in the context of thin disk hydromagnetic processes play a enigmatic role in collimation and acceleration of outflows/jets.

Blandford and Payne [1] (BP) assumed an axially symmetric, self-similar, cold magnetospheric flow originating from the Keplerian disc and asserted that a centrifugal pressure driven outflow is possible if the poloidal component of the magnetic field makes an angle less than 60° . At large distances from the disc, the toroidal component of the magnetic field becomes important and aides in collimation the outflow. Königl [27] in his work obtained radial self-similar configuration of magnetic field inside a cold and partially ionized disc and showed that for certain set of parameters BP type wind can be produced. Chakrabarti and Bhaskaran [8] provided more general approach to the solution of the field and obtained well collimated bipolar outflows and radio jets from magnetized accretion discs in self-consistent manner.

Another genre of magnetized disk solutions are present in the literature where the background flow is assumed to be the standard Keplerian disks and the magnetic field is assumed to be sheared and advected by the flow [24, 29, 41]. These works showed that discs with sufficient magnetic flux tube can eventually launch cosmic jets as the field structure close to disc surface becomes Blandford-Payne type. There exist few works that extends to Kerr black holes. The gravitomagnetic potential of a rotating black hole in the presence of a differentially rotating disk is seen to generate poloidal loop structures close to and in the ergosphere that may support extraction of rotational energy from the black hole [22, 23]. In principle the Kerr hole may even drive a self-excited dynamo and amplify weak (even axisymmetric) magnetic field to a higher field strength [25, 26]. A large body of

literature is present that explores many aspects of the effects of buoyancy and shear amplification on these magnetic flux in the paradigm of thin accretion disk (e.g., [9–11, 15, 16, 27, 40]).

All the works discussed above are in the paradigm of thin accretion disk or standard Keplerian disc. But now, we shall turn our attention to magnetized thick disc where due to the combined effect of magnetic tension and buoyancy, toroidal fields are ejected from the disc and may produce jets without having any significant poloidal component. If accretion rate is high ($\dot{M} \gg \dot{M}_{Edd}$), the radiation emitted by the in-falling matter exerts a significant pressure on the gas which inflates the disc making it geometrically ‘thick’ [$H(r) \sim r$]. Thick accretion discs have very little angular momentum and matter may fall into the central object without any need for a viscosity and also the thick accretion discs have funnels like openings or chimneys where the anisotropic radiation field could be sufficiently strong to accelerate radio jets. But still, magnetic fields can be observed in jets and this makes the ‘chimney’ region magnetically active. A thorough analytical study of the behaviour of toroidal magnetic flux tubes in the backdrop of thick accretion discs has been studied by Chakrabarti and D’Silva ([9]; hereafter CD94(I) and [12]; hereafter, CD94(II)). They showed that depending upon the various flows and field parameters, such as, initial position of release, cross-sectional radius of the flux tubes, angular momentum distribution, etc. flux rings injected into thick disc will emerge into the “chimney” (funnel like opening at the inner part of the disc) or will be expelled away. The magnetic fields are cannibalized along with the accreting matter from the companion and are sheared into forming toroidal flux tubes. From this study it can be observed that firstly, for sufficiently high disc temperature ($T_p > 4 \times 10^{10}$ K), the magnetic tension dominates over all other effects and the tube collapses catastrophically towards the axis and thus squeezing out matter in the disk along the axis of the black hole in the process to form radio jets. The sudden collapse of fields in the funnel would cause destruction of the inner part of the disc forming blobby radio jets. Detailed observation of GRS1915+105 shows these features (Mirabel and Rodriguez [32], Mirabel et al. [33], Nandi et al. [34]). Secondly, for proper entropy condition coronal structure is possible to form as flux tubes can oscillate inside the disc creating an internal structure similar to the solar interior. So far, no study of the flux tube behaviour and its possible effects on the flow dynamics and on the jet formation in the context of a self-consistent, time dependent, geometrically thick transonic flow has been performed. Hence, we first simulate a time dependent inviscid accretion disk using finite difference grid based numerical method. We, then, inject toroidal thin magnetic flux tube into the inviscid flow and follow its trajectory, its effect on the flow dynamics and its role in the collimation and acceleration of the outflow and jet.

2 Governing Equations for Hydrodynamic Flow and Flux Tubes

2.1 Hydrodynamic Equations

Equations governing hydrodynamic flow is comprised of the conservation laws, namely, the mass, momentum, and energy conservation. These equations can be written as, using dimensionless units that are presented in Ryu et al. [37, 38], Molteni et al. ([31], hereafter, MRC96), Giri et al. ([17], hereafter, GC10) and Giri [18] in great detail. For inviscid flow, hydrodynamic equations can be obtained from Navier-Stokes equation by ignoring viscous stress tensor. The equations are given as,

$$\frac{\partial \rho}{\partial t} + \nabla \cdot (\rho \mathbf{v}) = 0 \quad (1)$$

$$\rho \frac{\partial \mathbf{v}}{\partial t} + \rho (\mathbf{v} \cdot \nabla) \cdot \mathbf{v} = -\nabla p + \mathbf{f}_{\text{grav}} + \mathbf{f}_{\text{mag}} + \nabla \cdot \tau \quad (2)$$

$$\frac{\partial E}{\partial t} + \nabla \cdot \left[\left(H + \frac{1}{2} v^2 \right) \cdot \rho \mathbf{v} \right] = 0. \quad (3)$$

H is the enthalpy of the system, \mathbf{f}_{grav} and \mathbf{f}_{mag} are the gravitational force and the force due to magnetic field respectively. These two forces come under the broader classification of body forces. τ is the viscous stress tensor that has six mutually independent components but for thin accretion flow the most dominant contributor is $\tau_{r\phi}$ component (in cylindrical co-ordinate system) and thus we can ignore other components. For non magnetized inviscid flow we put $\tau = 0$ and $f_{\text{mag}} = 0$. Equations (1)–(3) can be written in terms of conservative variables in a compact form,

$$\frac{\partial \mathbf{q}}{\partial t} + \frac{1}{r} \frac{\partial (r \mathbf{F}_1)}{\partial r} + \frac{\partial \mathbf{F}_2}{\partial r} + \frac{\partial \mathbf{G}}{\partial z} = \mathbf{S}, \quad (4)$$

where the state vector is

$$\mathbf{q} = \begin{pmatrix} \rho \\ \rho v_r \\ \rho v_\theta \\ \rho v_z \\ E \end{pmatrix}, \quad (5)$$

the flux functions are

$$\mathbf{F}_1 = \begin{pmatrix} \rho v_r \\ \rho v_r^2 \\ \rho v_\theta v_r \\ \rho v_z v_r \\ (E + p)v_r \end{pmatrix}, \mathbf{F}_2 = \begin{pmatrix} 0 \\ p \\ 0 \\ 0 \\ 0 \end{pmatrix}, \mathbf{G} = \begin{pmatrix} \rho v_z \\ \rho v_r v_z \\ \rho v_\theta v_z \\ \rho v_z^2 + p \\ (E + p)v_z \end{pmatrix}, \tag{6}$$

and the source function is

$$\mathbf{S} = \begin{pmatrix} 0 \\ \frac{\rho v_\theta^2}{r} - \frac{\rho r}{2(\sqrt{r^2+z^2}-1)^2 \sqrt{r^2+z^2}} - f_{mag,r} \\ -\frac{\rho v_r v_\theta}{r} \\ -\frac{\rho z}{2(\sqrt{r^2+z^2}-1)^2 \sqrt{r^2+z^2}} + f_{mag,z} \\ -\frac{\rho(rv_r+zv_z)}{2(\sqrt{r^2+z^2}-1)^2 \sqrt{r^2+z^2}} \end{pmatrix}. \tag{7}$$

Here, the energy density (without potential energy) is given as(GC10, MRC96),

$$E = p/(\gamma - 1) + \rho(v_r^2 + v_\theta^2 + v_z^2)/2,$$

where ρ is the mass density, γ is the adiabatic index, p is the pressure, v_r , v_θ and v_z are the radial, azimuthal and vertical components of velocity respectively.

2.2 Equation of Motion of the Flux Tubes

We consider an azimuthally symmetric flux ring with the approximation that the cross sectional radius of the flux ring is smaller compared to local pressure scale height. This enables us to assume that variation of different physical quantities inside the tube is negligible. Here, following CD94(I), the equations of motion for

thin axisymmetric flux tube are given as,

$$\ddot{\xi} - \xi \dot{\theta} + \frac{X}{(1+X)} [-\xi \dot{\phi}^2 \sin^2 \theta - 2\xi \omega \dot{\phi} \sin^2 \theta] = \frac{X}{(1+X)} \left\{ \frac{M}{X} [g - \xi \omega^2 \sin^2 \theta] - T_{ens} \sin \theta - \frac{D_r}{\pi \sigma^2 \rho_e} \right\}, \quad (8)$$

$$\xi \ddot{\theta} + 2\dot{\xi} \dot{\theta} + \frac{X}{(1+X)} [-\xi \dot{\phi}^2 \sin \theta \cos \theta - 2\xi \omega \dot{\phi} \sin \theta \cos \theta] = -\frac{X}{(1+X)} \left\{ \frac{M}{X} \xi \omega^2 \sin \theta \cos \theta + T_{ens} \cos \theta + \frac{D_\theta}{\pi \sigma^2 \rho_e} \right\}, \quad (9)$$

$$\xi \sin \theta \ddot{\phi} + 2\dot{\xi} \sin \theta (\dot{\phi} + \omega) + 2\dot{\xi} \cos \theta \dot{\theta} (\dot{\phi} + \omega) + \xi \sin \theta \left\{ \dot{\xi} \frac{\partial \omega}{\partial r} + \dot{\theta} \frac{\partial \omega}{\partial \theta} \right\} = 0, \quad (10)$$

where, (ξ, θ, ϕ) is the position of a point inside a flux ring having magnetic field B . Here, ξ is measure of radial distance in the unit of Schwarzschild radius (r_g). Here, X is defined as $X = m_i/m_e$ where, $m_i = \rho_i \pi \sigma^2 \cdot 2\pi r \sin \theta$ is the mass inside the flux tube of radius of cross section (in the meridional plane) σ and $m_e = \rho_e \pi \sigma^2 \cdot 2\pi r \sin \theta$ is the mass of the external flow displaced by the flux tube. The flux $\psi = B\pi\sigma^2$ through the ring remains constant. The flux tube experiences buoyancy and the buoyancy factor is given by,

$$M = \frac{\rho_e - \rho_i}{\rho_e} = \frac{m_e - m_i}{m_e}$$

where ρ_e and ρ_i represent external and internal densities respectively. In case of flux tubes moving adiabatically with its surrounding we solve for ρ_i/ρ_e from the equation,

$$k_1 \left(\frac{\rho_i}{\rho_e} \right)^{4/3} + k_2 \left(\frac{\rho_i}{\rho_e} \right)^2 - 1 = 0, \quad (11)$$

where,

$$k_1 = \frac{(1 - \beta_e M_0)}{(1 - M_0)^{4/3}},$$

$$k_2 = \beta_e \frac{M_0}{(1 - M_0)^2} \left(\frac{T_e}{T_{e,0}} \right)^2 \left(\frac{\xi \sin \theta}{\xi_0 \sin \theta_0} \right)^2.$$

From the ratio ρ_i/ρ_e we calculate the magnetic buoyancy. The effective acceleration due to gravity is,

$$\mathbf{g}_{eff} = (g - \xi\omega^2 \sin^2 \theta)\hat{\xi} - \xi\omega^2 \sin \theta \cos \theta \hat{\theta} \quad (12)$$

where, g is given as $g = 1/2(\xi - 1)^2$ in Schwarzschild unit. The drag force per unit length is given as,

$$\mathbf{D} = -0.5C_D\rho_e\sigma|(\dot{\xi} - v)\hat{\xi} + \xi\dot{\theta}\hat{\theta}|(\dot{\xi} - v)\hat{\xi} + \xi\dot{\theta}\hat{\theta} \quad (13)$$

where, $C_D = 0.4$ is a dimensionless coefficient that has constant value of 0.4 for high Reynold's number, [19]. Magnetic tension force is given by

$$T_{ens} = \frac{4\pi M_0 T_e(\xi_0)}{\mu_e A(1 - M_0)\xi_0 \sin \theta_0}$$

is a dimensionless measure of the magnetic tension (CD94(I)) where, $T_e(\xi_0)$ is the initial of the external fluid, (ξ_0, θ_0) is the initial position of the flux tube, A is area increment factor given as $A = (\sigma/\sigma_0)^2$, where σ_0 is the initial cross sectional radius, σ is the instantaneous radius and M_0 is the initial buoyancy factor, which is calculated to be $M_0 = B^2/8\pi p_{g,e}$ where, $p_{g,e}$ is external gas pressure. As $A(t) = \sigma^2(t)/\sigma_0^2$, this gives the evolution of the flux tubes over the course of the simulation. Explicit form of this area expansion factor is given as (CD94(I)),

$$A = \left(\frac{T_e(\xi_0, \theta_0)}{T_e(\xi, \theta)} \right)^3 \left(\frac{\xi_0 \sin \theta_0}{\xi \sin \theta} \right) \left(\frac{1 - M_0}{1 - M} \right)$$

where, $T_e(\xi, \theta)$ is directly coming from our simulation at each instant of time.

For the purpose of simulation, we have considered the black hole to be a stellar mass black hole with the mass $10M_\odot$. Outer boundary of the disc is assumed to be at $200r_g$ although the actual size of the disc is much larger than what we have considered. Since we have considered an inviscid disc the angular momentum remains constant throughout the disc. For the detail description of the numerical setup for the inviscid disc simulation refer to [13]. For schemes, basic properties of the code, and different test results, please refer to [20], [38] and [37]. We inject the magnetic flux rings at the outer boundary near the equatorial plane ($\theta = 89^\circ$) with a initial magnetic buoyancy (M_0) which we calculate by taking the ratio between the magnetic pressure and external gas pressure. We use the injected flow to have constant specific angular momentum of (1) $\lambda = 1.6$, and (2) $\lambda = 1.7$ and for each of these cases we use the specific total energy $\varepsilon = 0.001, 0.002, 0.006$. For detailed set up of the magnetized disc refer to [14]. We couple the equations of motions for the flux tube with the hydrodynamic Total Variation Diminishing (TVD) code. We modify the source function as given in Eq.(7) by adding Lorentz force term. This will include flux tube's effect on the fluid. We calculate the density, velocity, pressure and temperature distribution using time dependant TVD code based on the

boundary values and the equation of state only. These flow parameters are used as the input parameters for computing a flux tube's evolution inside the disc since the drag, buoyancy etc. depend on the environment in which the tube is moving and those in turn are plugged in Eqs. (8)–(10) and we numerically solve them using the fourth order Runge-Kutta method.

3 Effects of Magnetic Flux Tube

The trajectories of the flux tubes are obtained in our simulations by solving the Eqs. (8)–(10) described in the Sect. 2.2 and are plotted in $r - z$ plane. Figure 1 shows the trajectories for the flux tubes injected with initial cross sectional radii $0.001, 0.005, 0.01, & 0.1 r_g$ respectively released from the outer boundary with two different flow energies, namely, $\varepsilon = 0.001, 0.002$ (marked). For both the energies, flux tubes having initial $\sigma < 0.1 r_g$ emerge in the chimney. Flux tubes with

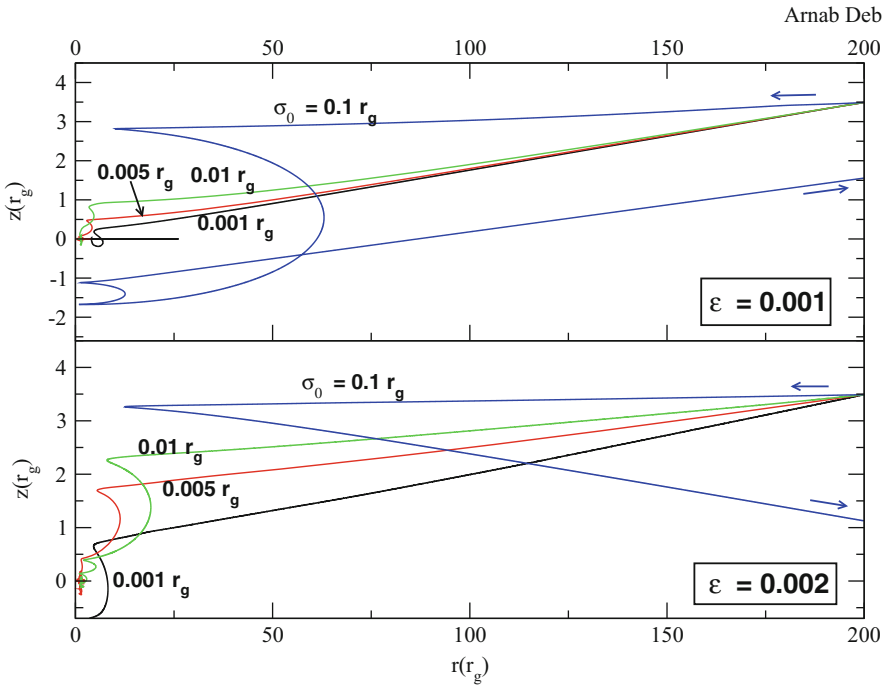


Fig. 1 Trajectories of flux tubes injected from the outer boundary i.e., $r = 200r_g$ and $\theta = 89^\circ$ with zero initial velocity. Trajectories are in $r = R \sin \theta$ vs. $z = R \cos \theta$ plane. The trajectories are drawn for a flow with angular momentum $\lambda = 1.6$ and energies 0.001 (upper panel) and 0.002 (lower panel). σ is the cross sectional radii of the injected flux tubes. Here σ values are $0.001 r_g, 0.005 r_g, 0.01 r_g$ and $0.1 r_g$ (Deb et al. [14])

$\sigma \geq 0.1r_g$ are expelled for the lower energy case. As we increase the energy of the flow, the flux rings tend to oscillate more as they will have more kinetic energy than the lower flow energy configuration. Since this is an inviscid flow, Coriolis force will not play any part in this and flux tubes will move inwards along the direction of local pressure gradient.

Jets can be categorized into two classes: (a) sustained and slow moving outflow originating from the post shock region and (b) blob of fast moving matter that squirted out due to sudden collapse of the inner part of the disc. The type (a) outflows are accelerated indirectly and the collimation of this jet reduces its lateral expansion retaining its initial energy. The cross-sectional area increases slowly with distance (along Z axis) and thus they are accelerated. Figure 2 shows the radial distribution of outflow rate for magnetized and non-magnetized flow having angular momentum 1.6 and from the plots it is quite evident that outflow coming out of magnetized flow is collimated by the presence of magnetic flux tube. Figure 3 shows the z-velocity difference of magnetized and non magnetized flow and it can be observed that in case of magnetized flow the velocity has increased significantly and thus it can be inferred that the outflow has been accelerated in presence of magnetic flux tube. If we increase the angular momentum to 1.7 only the limit for expulsion of flux tubes changes but overall nature of the outcome remains same. Here, we have only summarized our results but for detailed analysis refer to [14]

4 Conclusion

In earlier studies, such as CD94(I), CD94(II), simulations were carried out to study the dynamics of flux tubes in the backdrop of time independent thick disk [3, 35, 36]. In those earlier works, the conclusions can be summarized as, depending upon the position of release flux tubes can emerge into the chimney making it highly magnetically active region or can be expelled away. It is also possible to construct favourable entropy condition so that flux tubes can oscillate inside the disc around equipotential surface and thus consequently storing the flux tubes until they become enough buoyant to leave the system. In this present study, we inject a toroidal flux tube and follow its dynamics and its effect inside a time dependent two quadrant accretion flow after removing the reflection symmetry. In our simulation depending on its initial cross sectional radius and flow parameters such as angular momentum and energy flux tubes move toward the “chimney” or oscillate till it gets expelled away. We also find that in case of certain angular momenta and energies, firstly, the outflow rates ($\dot{M}(r)$) from both upper and lower quadrants increase significantly in comparison to the outflow rates with respect to the non-magnetic cases and secondly, the outflow rate is reaching its maximum value at much smaller radius, i.e., the spread of the outflow at the upper and lower boundaries has reduced significantly. We find that the difference of z component of velocity of magnetized and non magnetized flow becomes positive in a very narrow zone of outflowing region indicating the increase of velocity in the presence of magnetic field.

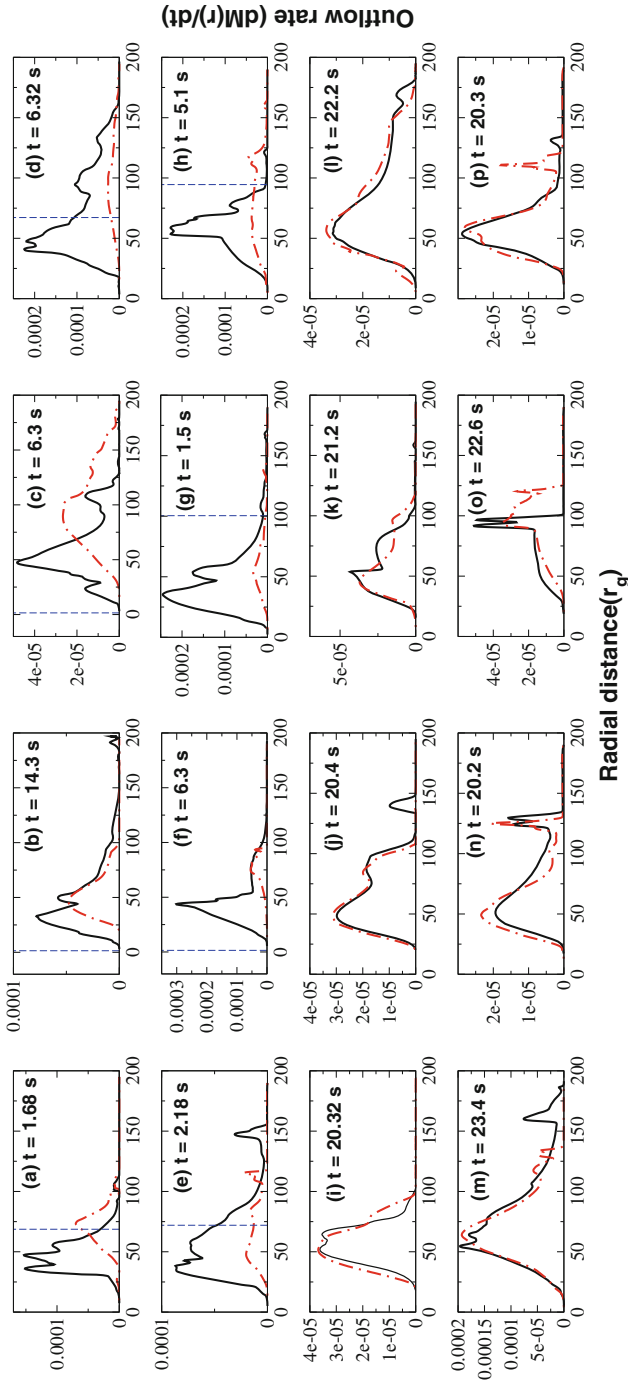


Fig. 2 Radial distribution of the outflow rate (\dot{M}_{out}) of the flow having the specific angular momentum (λ) = 1.6 and energy (ϵ) = 0.002. The black solid curve represents the outflow rate for the flow with magnetic field and red solid curve (dot-dashed in hard copies) denotes the result in non-magnetic case. The upper two rows (a)–(h) of the plot show the collimation of the outflow from upper and lower quadrants respectively for different flux tubes with different σ . The lower two rows (i)–(p) depict the dissipating effect once the flux tube has escaped or fallen into the black hole. The vertical dashed lines drawn in panels of first two rows depict the position of the flux tube at time for which the outflow rates are drawn (Deb et al. [14]) (Color figure online)

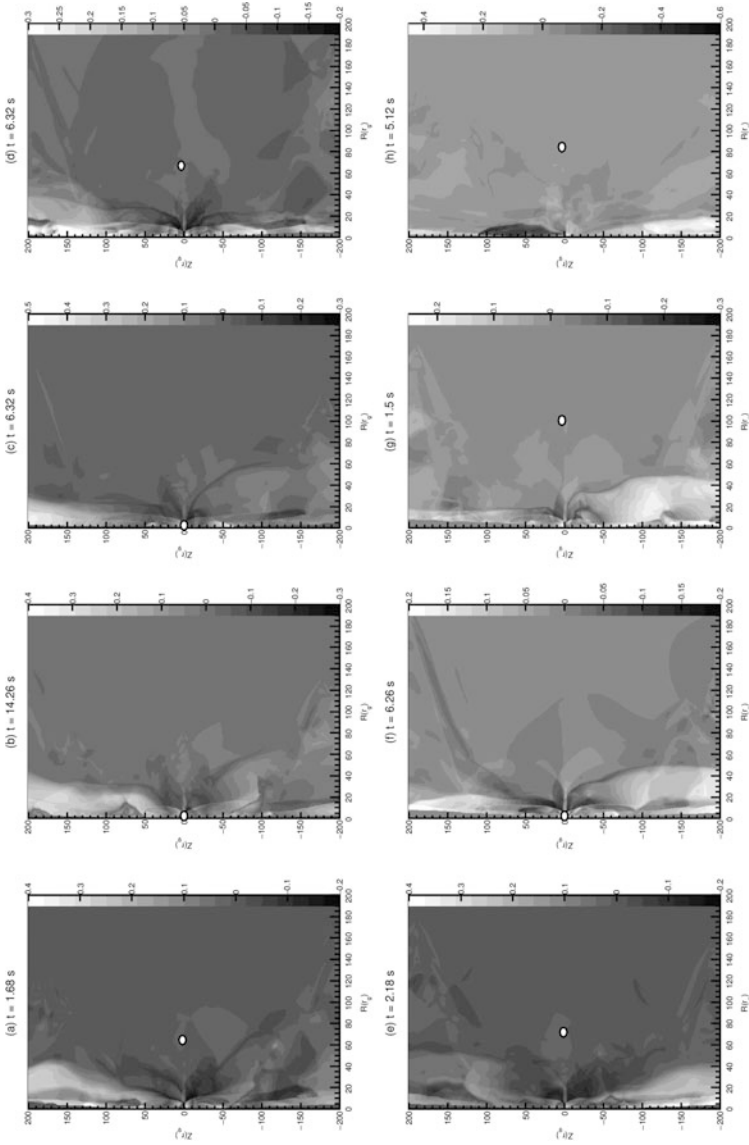


Fig. 3 Map of the difference between z -velocity of magnetized and non-magnetized flow. (a)–(d) represent the upper quadrant and (e)–(h) represent the lower quadrant of a two quadrant flow. Each pair of panels (upper and lower) represent different cross sectional radius. Here, σ ($= 0.001, 0.005, 0.01, 0.1 r_g$); Angular momentum (λ) is 1.6 and specific energy (ϵ) is 0.002. Each panel is drawn for different times were as the Fig. 2. The circles drawn in the panels give the position of flux tube at times for which the panels are drawn (Deb et al. [14])

References

1. Blandford, R.D., Payne, D.G.: *MNRAS* **199**, 883 (1982)
2. Camenzind, M.: In: Belvedere, G. (ed.) *Astrophysics and Space Science Library. Accretion Disks and Magnetic Fields in Astrophysics*, vol. 156, pp. 129–143 (1989). <https://doi.org/10.1007/978-94-009-2401-714>
3. Chakrabarti, S.K.: *ApJ* **288**, 1 (1985)
4. Chakrabarti, S.K.: *ApJ* **347**, 365 (C89) (1989)
5. Chakrabarti, S.K.: *Astron. Astrophys.* **351**, 185–191 (1999)
6. Chakrabarti, S.K., Titarchuk, L.G.: *Astrophys. J.* **455**, 623 (1995)
7. Chakrabarti, S.K., Titarchuk, L., Kazanas, D., Ebisawa, K.: *Astron. Astrophys. Suppl.* **120**, 163–166 (1996)
8. Chakrabarti, S.K., Bhaskaran, P.: *MNRAS* **255**, 255 (1992)
9. Chakrabarti, S.K., D’Silva, S.: *ApJ* **424**, 138 (1994)
10. Chakrabarti, S.K., Rosner, R., Vainshtein, S.I.: *Nature* **368**, 434 (1994)
11. Coroniti, F.V.: *ApJ* **244**, 587 (1981)
12. D’Silva, S., Chakrabarti, S.K.: *ApJ* **424**, 149 (1994)
13. Deb, A., Giri, K., Chakrabarti, S.K.: *MNRAS* **462**, 3502 (2016)
14. Deb, A., Giri, K., Chakrabarti, S.K.: *MNRAS* **472**(2), 1259–1271 (2017)
15. Eardley, D.M., Lightman, A.P.: *ApJ* **200**, 187 (1975)
16. Galeev, A.A., Rosner, R., Vaiana, G.S.: *ApJ* **229**, 318 (1979)
17. Giri, K., Chakrabarti, S.K., Samanta, M.M., Ryu, D.: *MNRAS* **403**, 516 (2010)
18. Giri, K.: In: Giri, K. (ed.) *Numerical Simulation of Viscous Shocked Accretion Flows Around Black Holes*. Springer Theses. Springer, Berlin (2015). ISBN 978-3-319-09539-4
19. Goldstein, S.: *Modern Developments in Fluid Mechanics*, vol. 1. Clarendon Press, Oxford (1938)
20. Harten, A.: *J. Comp. Phys.* **49**, 357 (1983)
21. Heyvaerts, J., Norman, C.: *ApJ* **347**, 1055 (1989)
22. Khanna, R.: *ASPC* **178**, 57 (1999)
23. Khanna, R.: (1999). arXiv:astro-ph/9903091
24. Khanna, R., Camenzind, M.: *Astron. Astrophys.* **263**, 401 (1992)
25. Khanna, R., Camenzind, M.: *A & A* **307**, 665 (1996)
26. Khanna, R., Camenzind, M.: *A & A* **313**, 1028 (1996)
27. Königl A.: *ApJ* **342**, 208 (1989)
28. Lovelace, R.V.E.: *Nature* **262**, 649 (1976)
29. Lovelace, R.V.F., Wang, J.C.L., Sulkanen, M.E.: *Astrophys. J.* **315**, 504 (1987)
30. Molteni, D., Lanzafame, G., Chakrabarti, S.K.: *ApJ* **425**, 161 (1994)
31. Molteni D., Ryu D., Chakrabarti, S.K.: *ApJ* **470**, 460 (1996)
32. Mirabel, I.F.; Rodríguez, L.F.: *Nature* **371**(6492), 46–48 (1994)
33. Mirabel, I.F., Rodríguez, L.F., Cordier, B., Paul, J., Lebrun, F.: *Nature* **358**(6383), 215–217 (1992)
34. Nandi, A., Chakrabarti, S.K., Vadawale, S.V., Rao, A.R.: *Astron. Astrophys.* **380**, 245–250 (2001)
35. Paczyński, B., Wiita, P.J.: *Astron. Astrophys.* **88**, 23 (1980)
36. Rees, M.J., Begelman, M.C., Blandford, R.D., Phinney, E.S.: *Nature* **295**, 17 (1982)
37. Ryu, D., Brown, G.L., Ostriker, J.P., Loeb, A.: *ApJ* **452**, 364 (1995)
38. Ryu D., Chakrabarti, S.K., Molteni, D.: *ApJ* **474**, 378 (1997)
39. Sakimoto P.J., Coroniti, F.V.: *ApJ* **342**, 49 (1989)
40. Shibata, K., Tajima, T., Matsumoto, R.: *ApJ* **350**, 295 (1990)
41. Wang, J.C.L., Sulkanen, M.E., Lovelace, R.V.: *Astrophys. J.* **355**, 38 (1990)